nature communications

Article

https://doi.org/10.1038/s41467-025-63654-1

Unraveling the role of viral interference in disrupting biennial RSV epidemics in northern Stockholm

Received: 9 September 2024

Accepted: 26 August 2025

Published online: 30 August 2025

Check for updates

Ke Li[1] ✉, Johan Hamrin[2], Anna Nilsson[3], Daniel M. Weinberger[1] & Virginia E. Pitzer[1]

Respiratory syncytial virus (RSV) primarily impacts infants and older adults, with seasonal winter outbreaks in temperate countries. Delayed RSV activity was reported worldwide during the 2009 influenza pandemic, and a disrupted biennial pattern of RSV activity was observed in northern Stockholm following the pandemic. Biennial patterns shifted to early/large outbreaks in even-numbered years and late/small outbreaks in odd-numbered years. However, the mechanisms underpinning this change in pattern remain unknown. In this work, we construct an age-stratified mechanistic model to explicitly test three factors that can lead to the change in RSV transmission dynamics: (1) birth rates, (2) temperatures, and (3) viral interference. By fitting the model to weekly RSV admission data over a 20-year period and comparing different models, we find that viral interference from influenza is the only mechanism that explains the shifted biennial pattern. We further demonstrate that the pandemic H1N1 virus has the strongest viral interference effects with RSV, aligning with a previous in vivo study. Our work demonstrates the complex interplay between different respiratory viruses, providing evidence that supports the presence of interactions between the H1N1 pandemic influenza virus and RSV at the population level, with implications for future public health interventions.

Respiratory syncytial virus (RSV) infections are a major public health concern for pediatric populations, older adults, and immunocompromised individuals[1,2]. In 2019, an estimated 100,000 deaths of children under the age of 5 were attributed to RSV globally[3]. RSV is highly seasonal, with winter epidemics in temperate countries. Biennial cycles of RSV activity have also been identified in Northern Europe and some states in the United States[4–9] In northern Stockholm, RSV activity shows a regular biennial pattern with early and large epidemics in odd-numbered seasons (e.g., 2001/02 season), and late and small epidemics in even-numbered seasons (e.g., 2002/03 season), influencing the risk of both lower respiratory infection and hospitalizations[10,11].

Disruptions to RSV epidemics were observed worldwide following the 2009 influenza pandemic, and delayed RSV activity was reported in the 2009/10 season[12–17]. In north Stockholm, our observations revealed an unexpected annual pattern for RSV epidemics during 2009-2011, characterized by large epidemics in two consecutive seasons. In particular, the biennial pattern of RSV epidemics completely shifted to early and large seasons in even-numbered years following the pandemic season. This disruption to the previous patterns provides an opportunity to understand factors that influence the annual and biennial epidemic cycles of RSV. To explain the change of RSV activity in northern Stockholm, we propose three hypotheses: (1) a sudden

[1]Department of Epidemiology of Microbial Diseases, Yale School of Public Health, New Haven, CT, USA. [2]Astrid Lindgren Children's Hospital, Karolinska University Hospital, Stockholm, Sweden. [3]Department of Women's and Children's Health, Division of Pediatric Oncology and Pediatric Surgery, Karolinska Institutet, Stockholm, Sweden. ✉e-mail: ke.li.kl662@yale.edu

increase of birth rates in 2009, (2) extremely low temperatures during the winters of 2009/10 and 2010/11, and (3) the occurrence of the 2009 influenza pandemic, which may interfere with RSV activity.

Mathematical models that explicitly depict the underlying mechanisms of virus transmission have advantages in being able to integrate heterogeneous mechanisms and test different hypotheses[18,19]. In this work, we started by analyzing weekly admission data for RSV from 1998 to 2018 in north Stockholm and demonstrated when and how RSV activity was disrupted in the area. We then constructed a mechanistic, age-stratified mathematical model that allows us to investigate different hypotheses for why the RSV biennial pattern may have shifted. Applying both a maximum likelihood method and a sampling-importance-resampling method, we estimated climatic and viral interference parameters and compared different models based on the hypotheses. Finally, we used the best-fit model to predict RSV dynamics under different scenarios, explaining how the number of susceptible individuals impacted RSV transmission.

Results

Disruption of temporal patterns of RSV

Hospitalizations for RSV, from July 1998 to June 2018, were strongly seasonal and showed an annual pattern of outbreaks occurring during the winter months in northern Stockholm (Fig. 1A, B). A biennial pattern was also detected, with early/large RSV epidemics in odd-numbered years (e.g., 1999/00 and 2001/02 years, highlighted in shaded areas, Fig. 1A) and late/small epidemics in even-numbered years (e.g., 2002/03 and 2000/01 years, Fig. 1A) prior to 2009. In odd-numbered years prior to the 2009 influenza pandemic, the mean timing (as indicated by the center of gravity) and the mean value of RSV activity intensity (as indicated by the peak value of RSV hospitalizations) were 31.2 weeks and 30.6 cases, respectively, compared to 35.7 weeks and 19.2 cases in even-numbered years (Fig. S1). However, we observed that the temporal pattern was disrupted during the 2009/10 and 2010/11 seasons. The timing of the biennial cycle exhibited a consistent pattern before 2009, but there was a sudden change in timing from 2009 to 2011 (Fig. 1C). The pattern shifted to early/large epidemics in even-numbered years and to late/small epidemics in odd-numbered years (highlighted in the shaded area, Fig. 1A) from 2010 to 2018. The timing of the annual cycle was consistent over time. These patterns can be quantified using the phase angle, which exhibits a shift in timing for the biennial cycles (black curve, Fig. 1C) around 2009 Following the pandemic, the mean timing and the mean value of RSV activity intensity are 35.2 weeks and 22.8 cases in odd-numbered years, respectively, compared to 31.5 weeks and 32 cases in even-numbered years (Figure S1).

Hypotheses for disrupted RSV dynamics

Having detected and quantified the disruption of RSV activity, we then sought to explore what factors led to the pattern change. The disrupted period (i.e., 2009–2011 years) coincided with three notable changes. The first observation was a sudden increase in the birth rate. By analyzing the annual birth rate data in northern Stockholm, we found that there was a 10% increase in the birth rate from 2010 to 2011 (Fig. S2A). We hypothesized that the increased birth rate would increase the size of the fully susceptible population, potentially affecting the RSV dynamics. Second, we observed that the area experienced exceptionally cold weather during the winters of 2010 and 2011 (Fig. S2B). We hypothesized that the cold weather could be associated with an increase in the transmission rate of RSV, leading to larger-than-expected epidemics in these years and a shift in the biennial pattern. Third, the occurrence of the H1N1 influenza pandemic during the 2009-2010 season resulted in extensive spread of the influenza virus before the typical RSV season (Fig. 2**, shaded pink**). There were two major waves observed in the catchment area; the first peak occurred in the week of September 14, while the second peak reached its maximum in the week of November 16. Based on experimental in vivo data from ferrets showing that infection with influenza could generate innate immune responses that temporarily prevent subsequent infection with RSV (but not vice versa), we hypothesized

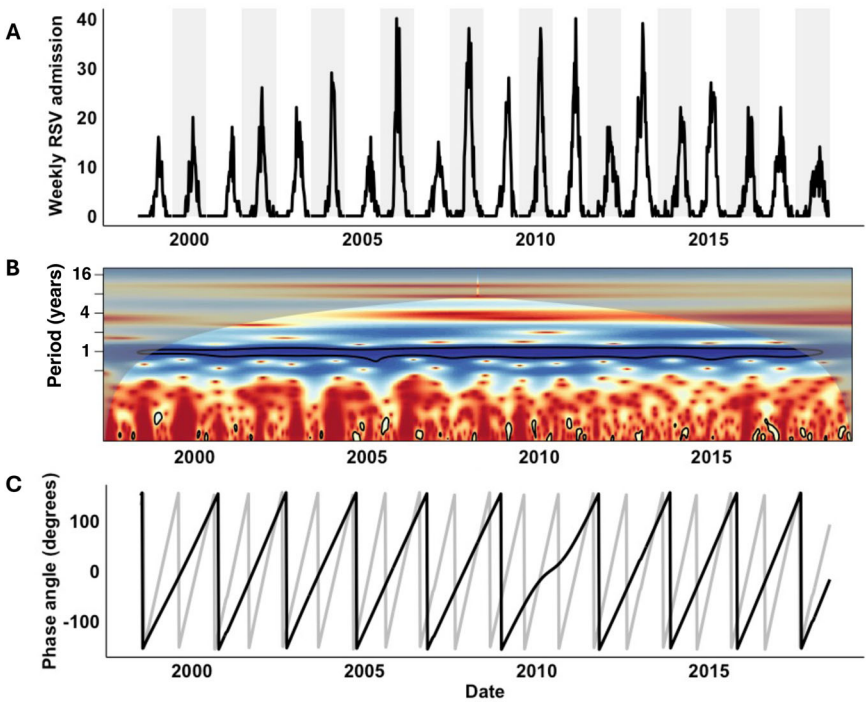

Fig. 1 | RSV epidemics in northern Stockholm. A Weekly hospital admissions due to RSV from July 1998 to June 2018 from the catchment area of Astrid Lindgren Children's Hospital in northern Stockholm. Odd-numbered seasons are highlighted in shaded areas. **B** The period (in years) of RSV epidemics. **C** The phase angle (in degrees) of the annual period (gray) and biennial period (black) of RSV epidemics. Source data are provided as a Source Data file.

https://doi.org/10.1038/s41467-025-63654-1

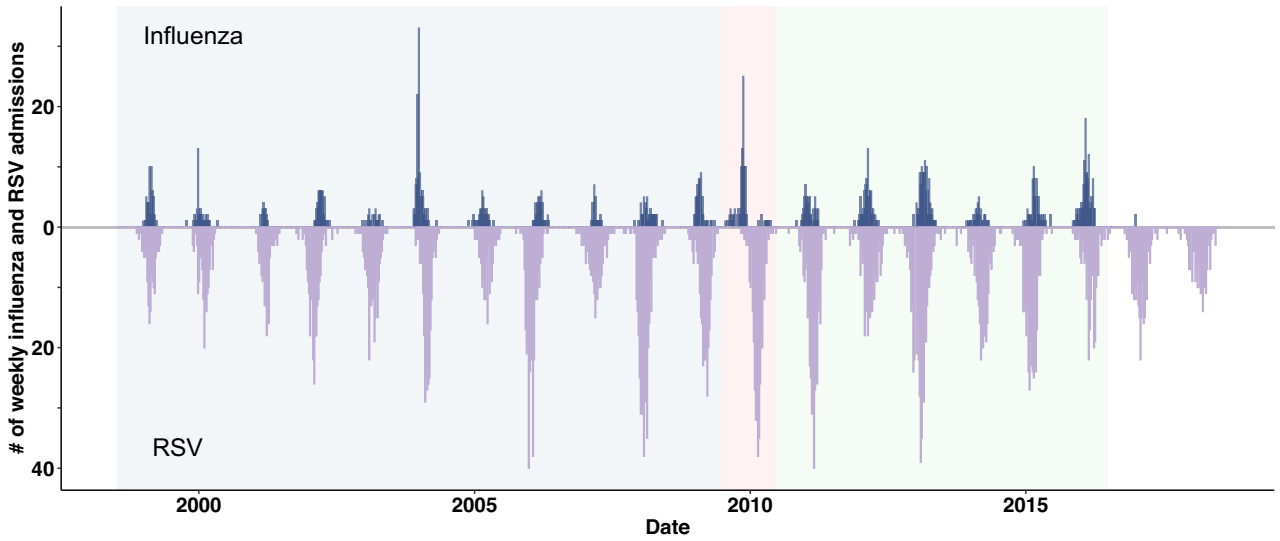

Fig. 2 | Influenza and RSV activity in northern Stockholm. Weekly hospital admissions due to influenza (above the horizontal line, in dark blue) or RSV (below the horizontal line, in purple) during the pre-pandemic period (1998–2009, shaded blue), the pandemic period (2009–2010, shaded pink), and the post-pandemic period (2010–2016, shaded green). Hospital admission data are only available for RSV for the years 2016–2018 (no background shading). Source data are provided as a Source Data file.

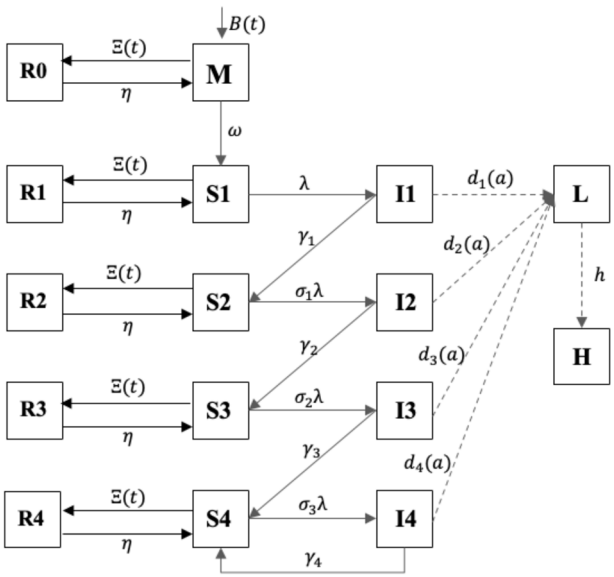

Fig. 3 | Transmission dynamic model for RSV. Model diagram illustrating the structure of the RSV transmission model (age is omitted for simplicity). Compartments *S1*-*S4* represent susceptible populations; compartments *I1*-*I4* represent infected populations, and compartments *R0*-*R4* represent temporarily-immune populations. Infants are born at rate $B(t)$ into the population with maternal antibodies that protect them from infection and disease, represented by *M*. Compartments *L* and *H* represent the population that develops severe lower respiratory infections and that is hospitalized, respectively; note that these two compartments represent observed states rather than infection states in the model. See **S1 Text** for detailed model equations.

that infection with influenza could result in temporary (innate) immunity to RSV infection, thereby disrupting RSV dynamics, particularly during the 2009/10 pandemic season[20]. The experimental viral interference effect was primarily observed when the interval between initiation of primary infection and subsequent challenge was <1 week and differed for the influenza A 2009 H1N1 pandemic strain compared to influenza A H3N2 and influenza B[21].

Dynamic model analyses

To explore the mechanistic relationship between these factors and the changes in the biennial pattern, we built an age-stratified SIS (Susceptible-Infectious-Susceptible) model for RSV transmission dynamics based on the model from Pitzer et al. [22], accounting for repeat infections (Fig. 3) and using natural history parameters derived from RSV cohort studies (S1 Table). See **Materials and Methods** for a detailed model description.

To explore whether the sudden increase in birth rates explains the biennial pattern change, we first calibrated the RSV transmission model to weekly RSV admissions from 1998 to 2008 (i.e., the seasons prior to the 2009 influenza pandemic) using a maximum likelihood method to estimate key parameters governing RSV transmission (see **Materials and Methods**). We then forward-simulated the model with the estimated parameters, using the observed data to parameterize the rate of birth into the maternal immunity state. We found that although the model could reproduce the biennial pattern before the disputed period (i.e., 1998–2009), it could not capture the altered biennial pattern of RSV epidemics after the pandemic season (i.e., 2009–2018, Fig. S3A, S2 Table).

Using the same approach, we incorporated the time-series of normalized temperatures and relative humidity data into the model by assuming the transmission rate varied in proportion to the climate factors, and we refitted the model to weekly RSV admissions from 1998–2008 and used the fitted model to predict RSV hospitalizations from 2009–2018. Again, we found that the model with both the observed changes to the birth rate and climatic factors could not capture the disrupted RSV epidemics after 2009 (Fig. S3B, S3 Table).

Next, we sought to investigate whether viral interference from influenza explains the change in the biennial pattern of RSV transmission. For this, we introduced temporary immune populations into the model (i.e., *R0*-*R4*, Fig. 3). We assumed that the temporary protection was mounted by influenza infection through the host innate immune response[20]. Here, we did not explicitly model the transmission dynamics for influenza due to increased model complexity and insufficient data on influenza subtypes. Instead, we used weekly influenza admissions data as model input and assumed that the conversion rate from susceptible (i.e., *S1*-*S4*) to temporarily immune was proportional to the number of recorded influenza admissions, such that

https://doi.org/10.1038/s41467-025-63654-1

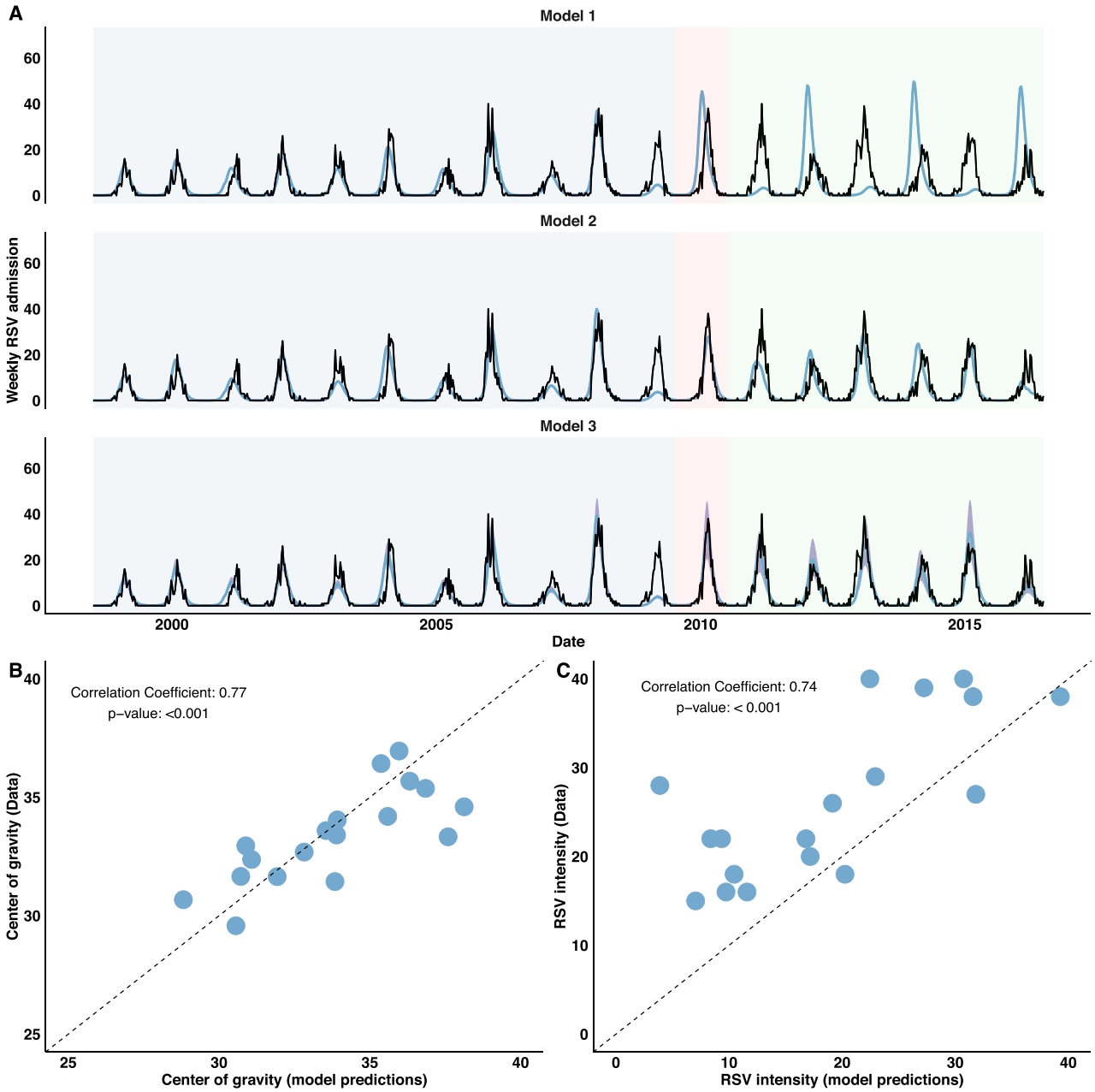

Fig. 4 | Model fit to RSV admissions to test different viral interference hypotheses. A Model fit (blue curve) to weekly RSV data (black curve) from 1998 to 2016, assuming viral interference effects are equivalent across different periods (i.e., Model 1: $\xi_s = \xi_p = \xi_{sp}$; see S5 Table for estimated parameter values), assuming viral interference effects differ before and after the pandemic (i.e., Model 2: ξ_s, $\xi_p = \xi_{sp}$; see S6 Table for estimated parameter values), or assuming viral interference effects differ across all three periods (i.e., Model 3: ξ_s, ξ_p, ξ_{sp}; see S7 Table for estimated parameter values). A 95% credible interval (CrI, shaded purple) was computed for the Model 3 using Latin Hypercube Sampling with Sampling-Importance-Resampling methods. Correlations between (**B**) the center of gravity (in weeks) and (**C**) the intensity of observed and predicted seasonal RSV epidemics (measured by the maximum weekly number of hospital admissions) from the best-fitting model—assuming viral interference effects differ across all three periods (Model 3)—were assessed using a two-sided Pearson correlation test (B: p-value = 9.2×10^{-4}, C: p-value = 2.1×10^{-4}). Source data are provided as a Source Data file.

$\Xi(t) = \xi_s flu_s(t) + \xi_p flu_p(t) + \xi_{sp} flu_{sp}(t)$. We assumed three parameters corresponding to viral interference effects during the pre-pandemic (1998–2009, ξ_s), pandemic (2009–2010, ξ_p), and post-pandemic (2010–2016, ξ_{sp}) periods. Notice that the post-pandemic influenza data was only available up to 2016. More explicitly, the three parameters ξ_s, ξ_p and ξ_{sp} represent viral interference effects from seasonal, pandemic, and co-circulating seasonal and pandemic influenza, respectively.

We further considered three scenarios: (1) viral interference effects are equivalent across different periods, i.e., $\xi_s = \xi_p = \xi_{sp}$; (2) viral interference effects differ before and after the pandemic, i.e., ξ_s, $\xi_p = \xi_{sp}$; and (3) viral interference effects differ across all three periods. We found that although Model 1 could reproduce the biennial pattern before the disputed period (i.e., 1998-2009, shaded blue, Fig. 4A), it could not capture the pattern change during the pandemic (i.e., 2009/2010, shaded red, Fig. 4A) and post-pandemic (i.e., 2010-2016, shaded green, Fig. 4A). Assuming different viral interference effects before and after the pandemic, we found that Models 2 and 3 could both successfully capture the observed RSV dynamics. The models were able to reproduce the shifted biennial

https://doi.org/10.1038/s41467-025-63654-1

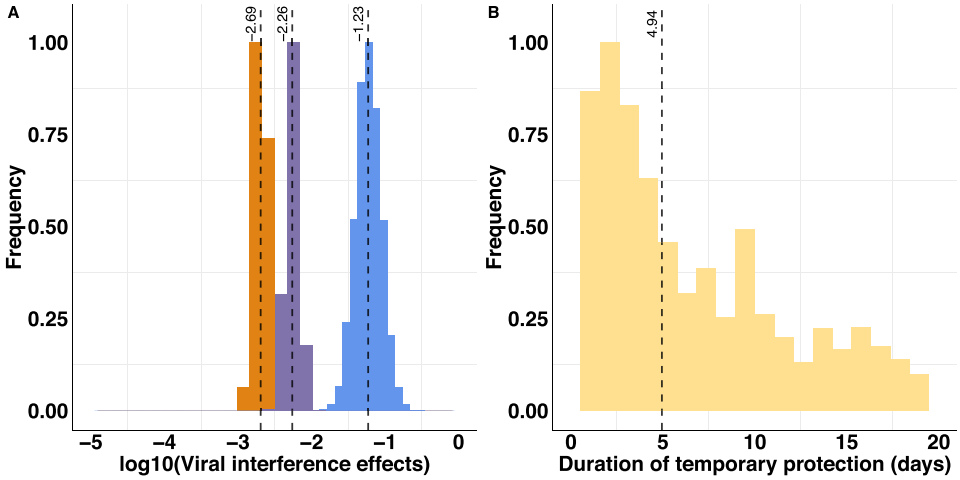

Fig. 5 | Estimated values for viral interference parameters. A The marginal distribution for the effect of viral interference parameters (on a log10-scale) before (ξ_s, in brown), during (ξ_p, in blue), and after (ξ_{sp}, in purple) the pandemic. The median estimate is indicated by a black dashed line. **B** The marginal distribution for the duration of viral interference parameter (η, in days).

pattern following the 2009/10 pandemic season, as observed in the data, showing late/small epidemics in odd-numbered years and early/large epidemics in even-numbered years (i.e., 2009-2016, shaded green, Fig. 4A). Notably, the models predicted two consecutive larger epidemics for the 2009/10 and 2010/11 seasons, as observed. Based on AIC scores, we found that Model 3, which assumes viral interference effects vary across all three periods, is the best-fitting model (S4 Table).

We then calculated the intensity and mean timing of RSV activity in each epidemic season for both observed and model-predicted data from different models. For the models without the viral interference effect, we found weak negative correlations between the observed and predicted center of gravity (Fig. S4A, S4C) and between the observed and predicted RSV intensity (Fig. S4B, S4D), indicating poor alignment between the data and model predictions. For the best-fitting model (Model 3), we found a strong positive correlation between the observed and predicted center of gravity of RSV epidemics (Fig. 4B, Pearson's correlation coefficient $r = 0.77$, $p < 0.001$) and between the observed and predicted RSV intensity (Fig. 4C, $r = 0.74$, $p < 0.001$). The results showed that the model with viral interference effects well represented the observed RSV dynamics and the shifted biennial patterns, suggesting viral interference from influenza had a significant role in impacting RSV transmission. We further investigated if incorporating climate factors into the viral interference model improved the model fit. However, we found that including temperature and relative humidity data did not enhance the model fit (S4 Table).

We also conducted a two-strain model analysis, explicitly modeling both RSV and influenza transmission dynamics and allowing for interaction between the two viruses during the pandemic and post-pandemic periods (see **Supplementary Materials**). The results were qualitatively consistent with those from the single-strain model. The most significant interference was estimated for the effect of pandemic influenza on susceptibility to RSV infection during the 2009 pandemic, leading to a shift in the RSV biennial transmission pattern, whereas we estimated little to no effect of RSV infection on susceptibility to influenza (consistent with the assumptions underlying the main analysis). This suggests that the key findings are robust to our modeling framework.

Parameter estimates suggest viral interference

To further quantify the uncertainty of viral interference parameters, we applied a Sampling-Importance-Resampling method to estimate credible intervals (CIs) of the parameters of interest (see **Materials and Methods**). The identified marginal distributions for viral interference parameters provided insight into the effect of viral interference (i.e., ξ_s, ξ_p, ξ_{sp}) and the duration of temporary protection (i.e., η) from influenza against RSV infection (Fig. 5). We found that the pandemic H1N1 influenza virus displayed the strongest viral interference effects with RSV (shown in blue, Fig. 5A). The median estimate for ξ_p (on a log10 scale) was −1.23, with a 95% CI of [−1.58, −0.89]. By contrast, we observed the weakest viral interference effect between seasonal influenza viruses and RSV before the pandemic period (ξ_s in brown, Fig. 5A), with a median estimate of −2.69 (95% CI: [−2.86, −2.52]). The median estimate for the viral interference effect after the pandemic (ξ_{sp} in purple, Fig. 5A), when co-circulation of seasonal and pandemic influenza viruses occurred, was intermediate at −2.26 (95% CI: [−2.43, −2.09]). In addition, the median estimate for the duration of temporary immunity was 4.94 days with a 95% CI of [0.55, 19.01] (Fig. 5B).

Linking susceptible population dynamics to RSV epidemics

Having demonstrated that the change of the RSV biennial pattern can be explained by viral interference from influenza, we then sought to understand how viral interference disrupted RSV epidemics. For this, we aggregated model-predicted time series of susceptible populations from 1998 to 2016 (i.e., *S1*, Fig. 6; S2–S4 see Fig. S5–S7) of all age groups from the best-fitting model (i.e., Model 3) with and without the viral interference effect. We found a temporal change of susceptible populations in the presence of viral interference during the pandemic season (shaded pink, Fig. 6A). The temporary conversion of the susceptible population (i.e., S1, Fig. 6A) to the temporarily-immune population (i.e., *R1*, Fig. 6B) delayed the availability of susceptible individuals for RSV infection, consequently delaying the RSV epidemic in the 2009/10 season (Fig. 6C). This also provided an explanation for the larger than expected RSV epidemic in the 2010/11 season, as there were more susceptible individuals after the pandemic season. Furthermore, we observed that the altered susceptible population dynamic did not revert to its pre-pandemic pattern, leading to the shifted biennial pattern for RSV transmission (Fig. 6C). Viral interference effects also exist between RSV and co-circulating pandemic and seasonal influenza, constantly converting the susceptible population to a temporarily immune population, but at a lower rate compared with the pandemic season (Fig. 6B, shaded green). However, it did not change the temporal pattern of the susceptible population (Fig. 6A), nor the RSV transmission pattern (Fig. 6C).

https://doi.org/10.1038/s41467-025-63654-1

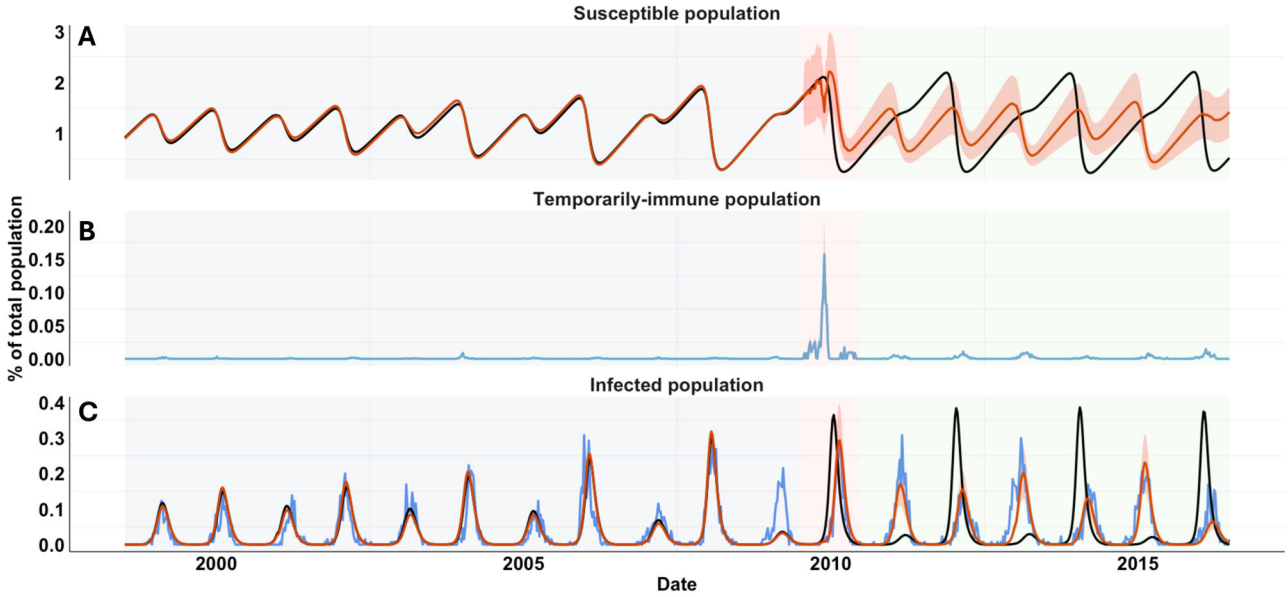

Fig. 6 | Model predictions of RSV epidemics and temporarily immune population. A Predicted time series of the fully susceptible population (*S1*) in the absence (black curve) or in the presence (red curve) of viral interference effects. **B** The predicted time series of the temporarily immune population (*R1*) is shown in blue. **C** Predicted time series of the primary infected population (*I1*) in the absence (black curve) or in the presence (red curve) of viral interference effects. Observed data are shown in blue. The 95% CrIs are shaded in orange. Predicted time series of partially susceptible (i.e., *S2-S4*), recovered (i.e., *R2-R4*), and reinfected populations (i.e., *I2-I4*) are provided in Fig. S5–S7. Source data are provided as a Source Data file.

Discussion

By analyzing the unexpected disruption of the biennial pattern of RSV epidemics in northern Stockholm, we found evidence supporting the presence of immunological interactions between the influenza virus and RSV[20,21] at the population level. Using an age-stratified dynamic transmission model for RSV, we assessed three hypotheses for the shift in the biennial pattern of RSV. We demonstrated that the sudden rise in birth rates and unusually cold temperatures in 2009/10 and 2010/11 could not explain the disruptions in RSV activity. Instead, only the model incorporating viral interference effects could successfully reproduce the observed RSV pattern change following the 2009 influenza pandemic, implying a significant role of viral interference from influenza in influencing RSV transmission. By applying both a maximum likelihood method and a sampling-importance resampling method, we estimated viral interference parameters, showing the presence of viral interference from influenza on subsequent RSV infection for a short period of time. In our previous work, we also demonstrated the presence of viral interference effects from influenza that impacted RSV epidemics following the 2009 influenza pandemic in the United States[23]. We further analyzed the model-predicted time series of susceptible populations, revealing that the change in the biennial pattern of RSV could be explained by temporary disruptions in the susceptible population.

Mechanistic models provide a valuable approach for dissecting underlying causal relationships among different compartments, integrating heterogeneous mechanisms, and studying various hypotheses. The presence of viral interaction between different viruses is evident at the host level[24–28]. In particular, within-host effects of viral interference from the pandemic H1N1 virus to subsequent RSV infection have been studied using a ferret model[20]. Here, by utilizing a mechanistic model and fitting it to the dataset capturing unusual disruptions of the biennial pattern of RSV, we demonstrated the impact of viral interference on RSV transmission at the population level.

One key finding from the model estimates is that the strongest viral interference effect was observed during the 2009/10 pandemic season, when the pandemic H1N1 virus was the predominant circulating influenza virus. In the post-pandemic seasons, the viral interference effects were stronger than in the pre-pandemic seasons, when only seasonal influenza circulated. This observation is likely due to a hierarchy of influenza viruses that induce different levels of temporary innate immunity. Laurie and colleagues, using a ferret model, demonstrated that the A(H1N1)pdm09 virus was most effective at inducing a temporary state of immunity, followed by the influenza B virus, and the A(H3N2) virus[21]. Although we could not study the interference effect of each subtype due to limited data, our results support the in vivo study and show that different subtypes could have varied interference effects with RSV, influencing RSV transmission in the population. They also showed limited interference from RSV against influenza infection, which is consistent with our assumption in the model[20]. Another key result from our model estimates is that temporary protection from viral interference to subsequent RSV infection is transient, lasting less than a week. This finding is consistent with another in vivo study[20], indicating that viral interference effects were only observed when the time interval between primary and challenge infections was less than 7 days.

Changes in birth rates have been shown to affect infectious disease dynamics. Models that incorporate changes in birth rates and vaccination levels can explain the complex transition from annual epidemics to irregular or multi-year cycles in measles incidence[29]. More generally, Morris et al. have shown that for diseases with high rates of loss of immunity, a change in birth rate will have negligible impact on the timing of epidemics[30]. Longer-term variations in birth rates may help explain changing patterns of RSV epidemics, such as the transition from a biennial pattern to an annual pattern during the 2000s in California, United States[22]. By contrast, our results showed that a temporary increase of birth rates in 2009 was not sufficient to explain the shift in the biennial pattern of RSV activity in northern Stockholm. Although there may be a delayed and/or long-term impact of birth rates on RSV dynamics, more work is needed to understand the causal relationship between birth rates and RSV transmission.

Using statistical or mathematical models, several studies have examined the relationship between climatic factors and RSV seasonality, and a significant association was found between temperature[31–36], potential evapotranspiration[22], vapor pressure[22], precipitation[22], and

relative/absolute humidity[34,37] and RSV activity in different geographic areas. In particular, Baker et al. demonstrated that local climate changes would influence the future dynamics of RSV epidemics, and the timing and intensity of RSV outbreaks would vary by location, influenced by the actual changes in climate[38]. Here, our results showed that the fluctuation of climatic variables, including temperatures and relative humidity, were not key factors responsible for the back-to-back large RSV epidemics in 2009/10 and 2010/11 seasons in northern Stockholm. Climatic factors alone could not reproduce the observed RSV pattern, and incorporating them into the viral interference model did not improve its ability to explain the data. It is possible that extreme temperatures in a single season might temporarily affect the timing of RSV activity, but they are unlikely to have a lasting impact on RSV transmission. Additional studies across different geographic settings could provide more insights into how different climatic factors affect RSV activity.

While our primary analysis employs a single-pathogen framework to successfully identify viral interference from pandemic influenza as the factor underpinning the change in the biennial pattern of RSV in Stockholm, we recognize the importance of evaluating whether a more flexible multi-strain approach would yield substantively different insights. A key trade-off between our single-strain and multi-strain models lies in balancing the simplicity of an explanation with mechanistic detail. Unlike the multi-strain model, the single-strain model can only be used to explore a single mechanism underlying the viral interference from influenza on RSV (i.e., reduced susceptibility or temporary immunity to RSV following influenza infection) and assumes no interference from RSV on influenza (consistent with the experimental data); furthermore, the viral interference parameter (i.e., ξ_s, ξ_p and ξ_{sp}) does not have a straightforward interpretation. However, we showed that the two-strain model provided qualitatively comparable results to the single-strain model, suggesting that both frameworks are capable of capturing the essential features of the observed dynamics driven by viral interference effects from influenza. While the multi-strain model allows for more explicit representation of potential interference mechanisms, it still requires strong assumptions about these mechanisms and more detailed input data, which is unavailable in our study (e.g., co-infection status). As such, we retain the single-strain model as our main framework due to better empirical support and comparable qualitative outcomes.

However, we acknowledge that viral interference can affect disease transmission at various levels, which could not be explicitly captured by the single-strain model. Specifically, interference may alter host susceptibility to secondary infection, by temporarily boosting immune defenses that protect against subsequent pathogens[20,39]. It can also reduce or enhance transmissibility during co-infection, as interactions between co-circulating viruses may suppress or amplify viral shedding, affecting how easily a host transmits one or both pathogens to others[40,41]. Additionally, interference can influence post-infection outcomes such as the severity of symptoms, the duration of illness, or the rate of recovery, potentially by modulating the host's immune response or by altering the dynamics of viral replication and clearance[21,42–44]. These effects may not be symmetric or unidirectional, and their manifestation can be highly context-dependent (e.g., household transmission[45]). The single-pathogen model can detect deviations in transmission consistent with external interference signals but cannot explicitly assess the causal mechanisms of such interference. Nevertheless, as richer and more granular data become available, particularly with direct measures of co-infections, the application of multi-pathogen models will be important for capturing the full spectrum of viral interference mechanisms.

There are some additional limitations to our study. First, we did not explicitly model RSV-A and RSV-B in this work due to data scarcity in northern Stockholm. It is possible that the interaction between RSV types A and B may help to explain some of the RSV transmission dynamics, as shown in[46]. However, differences in the predominant circulating subtype of RSV is unlikely to be the main driver of biennial patterns of RSV transmission[5,47,48]. We also did not have information on the different subtypes causing influenza hospital admissions; we therefore chose not to explicitly model the transmission dynamics of influenza, but instead we focus only on the effect of viral interference from influenza on RSV dynamics, as supported by the in vivo experimental data[20]. In addition, we did not have age information on the weekly admissions for RSV and influenza. Therefore, we assumed a well-mixed population and did not account for varying levels of immunity across different age groups beyond the age-specific contact matrices. We also tested a different model structure in which we assumed that only older age groups could be temporarily protected by influenza infection, but the model did not fit the data better.

The generalizability of single- or two-strain models relies on the assumption that the key mechanisms driving virus transmission—such as seasonal forcing, the depletion and replenishment of susceptible individuals, and temporary cross-protection or interference—are consistent across different settings. Our frameworks can yield useful insights when such mechanisms dominate and seasonal patterns are regular, as observed in northern Stockholm. However, in tropical or subtropical settings, where respiratory viruses often circulate year-round and exhibit multiple, irregular peaks, these assumptions may not hold. Moreover, the presence of multiple co-circulating virus types or subtypes, each with distinct dynamics and interaction patterns, adds further complexity. Generalizing the current modeling framework to other geographic regions or to viruses with more diverse subtype dynamics would likely require the inclusion of additional strains, heterogeneous transmission drivers, and region-specific climatic and behavioral covariates. Future work should aim to adapt the model for such settings by incorporating multi-pathogen frameworks and more flexible seasonal forcing structures that better capture local transmission patterns and interactions.

Understanding the impact of the dynamics of susceptible populations on the transmission of infectious diseases is critical for predicting and preparing for future outbreaks. By studying the unique biennial pattern change in northern Stockholm, our study demonstrated the complex interplay between different respiratory viruses and the implications for public health interventions. We highlighted that even a temporary, small disruption of the susceptible population caused by cross-protection mediated by viral interference effects led to a change in RSV activity. The delay in the RSV epidemic during the 2009/10 season was attributed to a temporary reduction in susceptible individuals, while the subsequent increase in susceptibility led to a larger epidemic in the 2010/11 season. Likewise, larger RSV outbreaks were observed after non-pharmaceutical interventions were relaxed following the COVID-19 pandemic[49–51]. A key implication of the association between the dynamics of susceptible populations and RSV transmission is that even a transient perturbation in susceptible populations could lead to a shifted pattern of disease transmission. This can be crucial for deploying and evaluating different vaccination strategies, and for assessing how vaccination coverage affects long-term disease patterns, contributing to informed decision-making in public health interventions.

Methods

Data sources

The original data collection was approved by the Swedish Ethical Review Authority. The current study does not involve research with human subjects, and written informed consent was waived by the Yale Institutional Review Board.

Data on the pediatric population in Northern Stockholm were obtained from the online base Statistics Sweden (https://www.statistikdatabasen.scb.se). The catchment area of the hospital includes the northern districts (Swedish: kommuner) of the Stockholm

region and approximately 51% (51.8% in 1998 and 50.7% in 2018) of the population residing in central Stockholm. The number of children (0-17 years) living in the catchment area increased from 201,334 in 1998 and to 265,268 in 2018. Of these, 5.6% were under 1 year old, 23.1% were aged 1–4 years, 28.9% were aged 5–9 years, and 42.4% were aged 10–17 years.

Astrid Lindgrens Children's Hospital at Karolinska Hospital Solna, is a tertiary referral university hospital with a pediatric intensive care unit (with 6–10 beds during this time frame) and an extracorporeal membrane oxygenation center (with 2–4 beds). The neonatal intensive care unit is a regional referral unit for babies from gestational age 22+ weeks. The emergency department had approximately 48,000-50,000 visits/year in the later time periods. The number of hospital beds varied between 150-190 over the study period.

The number of live births in the population residing in the hospital's catchment area was approximately 10,750 in 1998 and 14,832 in 2018. The birth clinic at Karolinska University Hospital in Solna has approximately 2500 live births per year and prioritizes high-risk births. There are 3 more birth clinics at other hospitals in Stockholm, and another, smaller birth clinic opened and closed during the study period.

Stockholm experienced the first wave of the 2009 Influenza A (H1N1) pandemic at the end of summer 2009, with a total of 15 pediatric admissions at Astrid Lindgren Children's Hospital from mid-July until mid-September. After a three-week hiatus, pediatric admissions resumed in early October, peaking in mid-November before declining sharply, with the last admission occurring in early December. In total, 77 children were hospitalized during the second wave of the 2009 Influenza A (H1N1) outbreak. The impact of the pandemic on hospitalized children in Stockholm has also been described in relation to co-circulating viral infections and within the context of a 16-year span of influenza epidemics[52,53].

Clinical data

Positive viral findings of RSV and influenza virus among pediatric patients (under 18 years old) were provided by the Karolinska University Hospital Virology unit and matched to medical records. Virus detection was performed on samples from nasopharyngeal aspirates. In the first period of the study (1998–2007), viral detection of RSV and influenza virus was performed using immunofluorescence. In the second period of the study (2008–2018), viruses were detected with a rapid-antigen test (RSV only) or through PCR (RSV and influenza virus). Improved sensitivity of viral testing in the second study period leads to an increased number of cases among older children, as they have lower viral loads compared to young children. From the matched medical records, the following data were extracted for each virologically confirmed case: the duration of hospitalization, age and sex of the patient, underlying diseases (i.e., healthy, asthma, neuromuscular disease, immunosuppression, prematurity, chronic respiratory diseases, metabolic and gastrointestinal diseases), and disease severity. Based on medical records, only cases with positive findings and ongoing clinical signs of infection were included in the study. If the same child was admitted more than once during a 4-week span and still tested positive for RSV or influenza virus, only the first episode was included. Only cases where the primary address of the patient was within the Astrid Lindgren Children's Hospital catchment area were included.

Demographic data

We used the smooth.spline function (with 10 degrees of freedom) implemented in R (version 4.3.2) to interpolate weekly birth rates. Within our transmission model, we divided the <1 year age class into 12-month age groups to more accurately capture aging among this age class. The remaining population was divided into 9 age classes: [1,2) years, [2,3) years, [3,4) years, [4,5) years, 5–9 years, 10–19 years, 20–39 years, 40–59 years and 60 years old and above. We estimated the net rate of immigration/emigration for each age group (detailed in **S1 Text**) to produce a rate of population growth and age structure similar to that of northern Stockholm. Data on age-specific contact rates were obtained from[22] specifically, we used the POLYMOD contact matrix from the Netherlands, which had a similar contact pattern as Sweden.

Climatic data

The climatic variables used in this study were weekly temperature (in Celsius) and relative humidity (as a percentage) from July 1998 to June 2018. Weekly averages were calculated from the daily data. To incorporate the climate data into the RSV transmission model, we normalized the data to between −1 and 1.

The center of gravity and the intensity of RSV activity

The center of gravity of RSV activity for each season (G_s) was measured as the mean epidemic week, with each week weighted by the weekly number of admissions ($Y_{s,w}$), such that

$$G_s = \sum_{w\in[1:52]} w \times Y_{s,w} / \sum_{w\in[1:52]} Y_{s,w} \quad (1)$$

where w is an index for the week of each epidemic season, s. The center of gravity is a measure of the mean epidemic week, indicating the average timing of RSV activity. This measure has been used repeatedly in the literature for RSV and other pathogens[9,22,54–56]. The intensity of RSV activity for each season was determined by the maximum weekly number of hospitalizations. The rationale for using the maximum values is to capture the contrast between large and small epidemics observed in the data.

Wavelet analysis

We obtained the timing of RSV epidemics in each season based on phase decomposition obtained from wavelet analysis[57,58]. In the wavelet analysis, we used the 0.8–1.5 year and 1.5-2.5 year periodicity bands from the wavelet spectrum to extract weekly phase angles for the annual period and the biennial period, respectively.

Dynamic model description

Here, we used an age-stratified SIS (Susceptible-Infectious-Susceptible) model for RSV transmission dynamics. The model was proposed by Pitzer et al. [22] to study the environmental drivers of the spatio-temporal dynamics of RSV in the US. The model assumed individuals are born with protective maternal immunity, which wanes exponentially, leaving the infants susceptible to infection. We assumed a progressive build-up of immunity following up to four previous infections, based on data from birth cohort studies. Following infection with RSV, individuals develop partial immunity, reducing the rate of subsequent infection and relative infectiousness of the following infections. We also assumed that subsequent infections have a shorter recovery time compared to the primary infection. The model was described by a system of ordinary differential equations; see **S1 Text** for details.

As a sensitivity analysis, we also used a two-strain mechanistic model (Fig. S9) to assess its compatibility with our original single-strain model. We used an SIRS (Susceptible-Infectious-Recovered-Susceptible) model for influenza transmission dynamics and integrated the model into the RSV transmission dynamic model described above.

In the model, influenza dynamics are coupled to the RSV transmission model (Fig. 3) through two alternative interference pathways. First, we allow prior infection with one virus to change susceptibility to the other by a factor θ. Second, we allow coinfected individuals to have altered infectiousness at a rate ξ compared to infection with either virus, capturing changes in viral shedding when both pathogens are present.

We calibrated the two-strain model to both weekly RSV and influenza admissions from July 2009 to June 2016. We assumed the RSV parameters were fixed at their pre-pandemic estimates (see

Parameter estimation below). We estimated six influenza transmission parameters: a seasonal amplitude parameter, a seasonal offset parameter, a baseline transmission rate parameter, a reporting fraction parameter to scale infections with influenza to hospitalized cases, duration of influenza immunity, duration of influenza infection, and four viral interference parameters. We estimated these parameters using a maximum likelihood approach, assuming the number of hospitalizations during each week was Poisson distributed with a mean equal to the model-predicted number times the estimated reporting fraction. Other parameter values are provided in S1 Table. The full two-strain model structure, its detailed description, and model results are included in the **Supplementary Materials**.

Parameter estimation

For the single-strain model without viral interference, we first fitted the transmission dynamic model for RSV to weekly RSV admissions from July 1998 to June 2008 (i.e., 11 seasons before the influenza pandemic). We estimated four parameters: a seasonal amplitude parameter (α), a seasonal offset parameter (ϕ), a baseline transmission rate parameter (β_0), a reporting fraction parameter (f) to scale RSV low respiratory disease cases to hospitalized cases. For the model testing the climate hypothesis, we estimated two additional parameters, including the seasonal amplitude parameters for temperatures (α_{Temp}) and relative humidity (α_{RelHum}). The force of infection is given by:

$$\lambda = \beta_0(1+\alpha\cos(2\pi vt-\phi)+\alpha_{Temp}\times Temp+\alpha_{RelHum}\times RelHum)I^*, \quad (2)$$

where $Temp$ and $RelHum$ are normalized data of temperatures and relative humidity, and I^* denotes all infection states. Note that we assumed $\alpha_{Temp}=\alpha_{RelHum}=0$ when testing the birth rate hypothesis. We estimated these parameters using a maximum likelihood approach, assuming the number of hospitalizations during each week was Poisson-distributed with a mean equal to the model-predicted number times the estimated reporting fraction. Other parameter values for the model were adopted from ref. 22, and they are provided in S1 Table. We seeded the model with one RSV-infected individual in each age group except the <1 year group, then used a burn-in period of 47 years to ensure the model reached a quasi-equilibrium steady state.

For the models with viral interference, we fitted the transmission dynamic model for RSV to weekly RSV admissions from July 1998 to June 2016 (i.e., all seasons across the study period for which we had influenza admissions data). We first estimated the parameters for RSV transmission (i.e., β_0,α,ϕ,f) and viral interference parameters using a maximum likelihood approach. We also estimated climatic parameters (i.e., α_{Temp}, α_{RelHum}) when all three factors (the observed birth rate change, climatic factors, and viral interference) were included. We determined the best model using Akaike Information Criterion (AIC) scores. To further quantify the uncertainty of viral interference parameters in the best-fitting model, we then applied a Sampling-Importance-Resampling method to estimate credible intervals (CIs) of those parameters. We used Latin Hypercube Sampling (LHS) to generate representative samples from a wide range of values for the parameter space $\Phi=(\xi_s,\xi_p,\xi_{sp},\eta)$. We drew 100,000 samples from a uniform distribution $U(-5,-1)$ for $\log_{10}(\xi_s,\xi_p,\xi_{sp})$, and from a uniform distribution $U(1,20)$ days for η. Note that we drew samples using a log10-scale for the ξ parameters because we had no prior knowledge of the magnitude of these parameters. To enhance computational efficiency, we used informative priors for the RSV transmission parameters (i.e., β_0,α,ϕ,f), setting their mean values to the estimates from the maximum likelihood approach and assuming a small variance, such that $\beta_0\sim N(8.51,0.5)$, $\alpha\sim N(0.27,0.1)$, $\beta_0\sim N(3.24,0.5)$, $f\sim U(0,1)$. Then, we generated forward simulations using the sampled parameter sets and fitted them to weekly RSV admissions from 1998 to 2016. We calculated the log-likelihoods of the model under each parameter set, assuming the number of hospitalizations during each week was Poisson-distributed with a mean equal to the model-predicted number times the estimated reporting fraction. We then normalized the log-likelihoods to assign weights to each parameter set and resampled (with replacement) 10,000 parameters from the joint distribution based on the weights.

Reporting summary

Further information on research design is available in the Nature Portfolio Reporting Summary linked to this article.

Data availability

The hospitalization data, along with demographic and climatic data in Sweden used in this study are publicly available on Github: https://github.com/keli5734/Sweden_study. Source data are provided with this paper.

Code availability

We used the R statistical software (v4.0.2) for all statistical analyses and visualization. Code used in this study is publicly available on Github: https://github.com/keli5734/Sweden_study, and archived at Zenodo with the https://doi.org/10.5281/zenodo.16740279.

References

1. Tin Tin Htar, M., Yerramalla, M. S., Moïsi, J. C. & Swerdlow, D. L. The burden of respiratory syncytial virus in adults: a systematic review and meta-analysis. *Epidemiol. Infect.* **148**, e48 (2020).
2. Shi, T. et al. Global, regional, and national disease burden estimates of acute lower respiratory infections due to respiratory syncytial virus in young children in 2015: a systematic review and modelling study. *Lancet* **390**, 946–958 (2017).
3. Li, Y. et al. Global, regional, and national disease burden estimates of acute lower respiratory infections due to respiratory syncytial virus in children younger than 5 years in 2019: a systematic analysis. *Lancet* **399**, 2047–2064 (2022).
4. Mlinaric-Galinovic, G. et al. The biennial cycle of respiratory syncytial virus outbreaks in Croatia. *Virol. J.* **5**, 18 (2008).
5. Waris, M. Pattern of respiratory syncytial virus epidemics in Finland: two-year cycles with alternating prevalence of groups A and B. *J. Infect. Dis.* **163**, 464–469 (1991).
6. Berner, R., Schwoerer, F., Schumacher, R. F., Meder, M. & Forster, J. Community and nosocomially acquired respiratory syncytial virus infection in a German paediatric hospital from 1988 to 1999. *Eur. J. Pediatr.* **160**, 541–547 (2001).
7. Weigl, J. A. I., Puppe, W. & Schmitt, H. J. Seasonality of respiratory syncytial virus-positive hospitalizations in children in Kiel, Germany, over a 7-year period. *Infection* **30**, 186–192 (2002).
8. Duppenthaler, A., Gorgievski-Hrisoho, M., Frey, U. & Aebi, C. Two-year periodicity of respiratory syncytial virus epidemics in Switzerland. *Infection* **31**, 75–80 (2003).
9. Bloom-Feshbach, K. et al. Latitudinal variations in seasonal activity of influenza and respiratory syncytial virus (RSV): a global comparative review. *PLoS One* **8**, e54445 (2013).
10. Eriksson, M., Bennet, R., Rotzén-Östlund, M., von Sydow, M. & Wirgart, B. Z. Population-based rates of severe respiratory syncytial virus infection in children with and without risk factors, and outcome in a tertiary care setting. *Acta Paediatr.* **91**, 593–598 (2002).
11. Reyes, M., Eriksson, M., Bennet, R., Hedlund, K.-O. & Ehrnst, A. Regular pattern of respiratory syncytial virus and rotavirus infections and relation to weather in Stockholm, 1984-–1993. *Clin. Microbiol. Infect.* **3**, 640–646 (1997).
12. Casalegno J. S., et al Impact of the 2009 influenza A(H1N1) pandemic wave on the pattern of hibernal respiratory virus epidemics, France, 2009. Euro Surveill. 2010;15. Available: https://www.ncbi.nlm.nih.gov/pubmed/20158981.

13. Meningher, T. et al. Relationships between A(H1N1)pdm09 influenza infection and infections with other respiratory viruses. *Influenza Other Respir. Viruses* **8**, 422–430 (2014).
14. Hirsh, S. et al. Epidemiological changes of respiratory syncytial virus (RSV) infections in Israel. *PLoS One* **9**, e90515 (2014).
15. Schnepf, N. et al. High burden of non-influenza viruses in influenza-like illness in the early weeks of H1N1v epidemic in France. *PLoS One* **6**, e23514 (2011).
16. Mak, G. C., Wong, A. H., Ho, W. Y. Y. & Lim, W. The impact of pandemic influenza A (H1N1) 2009 on the circulation of respiratory viruses 2009-2011. *Influenza Other Respir. Viruses* **6**, e6–e10 (2012).
17. Yang, L. et al. Impact of the 2009 H1N1 pandemic on age-specific epidemic curves of other respiratory viruses: a comparison of pre-pandemic, pandemic and post-pandemic periods in a subtropical city. *PLoS One* **10**, e0125447 (2015).
18. Grassly, N. C. & Fraser, C. Mathematical models of infectious disease transmission. *Nat. Rev. Microbiol* **6**, 477–487 (2008).
19. Pinky, L. & Dobrovolny, H. M. Epidemiological consequences of viral interference: a mathematical modeling study of two interacting viruses. *Front Microbiol* **13**, 830423 (2022).
20. Chan, K. F. et al. Investigating viral interference between Influenza A Virus and human respiratory syncytial virus in a ferret model of infection. *J. Infect. Dis.* **218**, 406–417 (2018).
21. Laurie, K. L. et al. Interval between infections and viral hierarchy are determinants of viral interference following influenza virus infection in a Ferret model. *J. Infect. Dis.* **212**, 1701–1710 (2015).
22. Pitzer, V. E. et al. Environmental drivers of the spatiotemporal dynamics of respiratory syncytial virus in the United States. *PLoS Pathog.* **11**, e1004591 (2015).
23. Li K., Thindwa D., Weinberger D. M., Pitzer V. E. The role of viral interference in shaping RSV epidemics following the 2009 H1N1 influenza pandemic. medRxiv. 2024. https://doi.org/10.1101/2024.02.25.24303336
24. Haney, J. et al. Coinfection by influenza A virus and respiratory syncytial virus produces hybrid virus particles. *Nat. Microbiol* **7**, 1879–1890 (2022).
25. Wu, A., Mihaylova, V. T., Landry, M. L. & Foxman, E. F. Interference between rhinovirus and influenza A virus: a clinical data analysis and experimental infection study. *Lancet Microbe* **1**, e254–e262 (2020).
26. Cheemarla N. R., et al. Dynamic innate immune response determines susceptibility to SARS-CoV-2 infection and early replication kinetics. *J. Exp. Med.* 2021;218. https://doi.org/10.1084/jem.20210583.
27. Swets, M. C. et al. SARS-CoV-2 co-infection with influenza viruses, respiratory syncytial virus, or adenoviruses. *Lancet* **399**, 1463–1464 (2022).
28. Czerkies M., Kochańczyk M., Korwek Z., Prus W., Lipniacki T. RSV protects bystander cells against IAV infection by triggering secretion of type I and type III interferons. bioRxiv. 2022. https://doi.org/10.1101/2021.10.11.463877.
29. Earn, D. J., Rohani, P., Bolker, B. M. & Grenfell, B. T. A simple model for complex dynamical transitions in epidemics. *Science* **287**, 667–670 (2000).
30. Morris, S. E. et al. Demographic buffering: titrating the effects of birth rate and imperfect immunity on epidemic dynamics. *J. R. Soc. Interface* **12**, 20141245 (2015).
31. Stensballe, L. G., Devasundaram, J. K. & Simoes, E. A. Respiratory syncytial virus epidemics: the ups and downs of a seasonal virus. *Pediatr. Infect. Dis. J.* **22**, S21–S32 (2003).
32. Paiva, T. M. et al. Shift in the timing of respiratory syncytial virus circulation in a subtropical megalopolis: implications for immunoprophylaxis. *J. Med Virol.* **84**, 1825–1830 (2012).
33. du Prel, J.-B. et al. Are meteorological parameters associated with acute respiratory tract infections?. *Clin. Infect. Dis.* **49**, 861–868 (2009).
34. Lapeña, S. et al. Climatic factors and lower respiratory tract infection due to respiratory syncytial virus in hospitalised infants in northern Spain. *Eur. J. Epidemiol.* **20**, 271–276 (2005).
35. Noyola, D. E. & Mandeville, P. B. Effect of climatological factors on respiratory syncytial virus epidemics. *Epidemiol. Infect.* **136**, 1328–1332 (2008).
36. Meerhoff, T. J., Paget, J. W., Kimpen, J. L. & Schellevis, F. Variation of respiratory syncytial virus and the relation with meteorological factors in different winter seasons. *Pediatr. Infect. Dis. J.* **28**, 860–866 (2009).
37. Welliver, R. The relationship of meteorological conditions to the epidemic activity of respiratory syncytial virus. *Paediatr. Respir. Rev.* **10**, 6–8 (2009).
38. Baker, R. E. et al. Epidemic dynamics of respiratory syncytial virus in current and future climates. *Nat. Commun.* **10**, 5512 (2019).
39. Piret, J. & Boivin, G. Viral interference between respiratory viruses. *Emerg. Infect. Dis.* **28**, 273–281 (2022).
40. Goto, H. et al. Enhanced growth of influenza A virus by coinfection with human parainfluenza virus type 2. *Med Microbiol Immunol.* **205**, 209–218 (2016).
41. Gonzalez A. J., Ijezie E. C., Balemba O. B., Miura T. A. Attenuation of Influenza A Virus Disease severity by viral coinfection in a mouse model. *J Virol.* 2018;92. https://doi.org/10.1128/JVI.00881-18.
42. Zhang, A. J. et al. Coinfection by severe acute respiratory syndrome Coronavirus 2 and influenza A(H1N1)pdm09 virus enhances the severity of pneumonia in golden Syrian hamsters. *Clin. Infect. Dis.* **72**, e978–e992 (2021).
43. Nickbakhsh, S. et al. Virus-virus interactions impact the population dynamics of influenza and the common cold. *Proc. Natl Acad. Sci. USA* **116**, 27142–27150 (2019).
44. Achten, N. B. et al. Interference between respiratory syncytial virus and human Rhinovirus infection in infancy. *J. Infect. Dis.* **215**, 1102–1106 (2017).
45. Ibiebele, J. C. et al. The role of viral interaction in household transmission of symptomatic influenza and respiratory syncytial virus. *Nat. Commun.* **16**, 1249 (2025).
46. White, L. J., Waris, M., Cane, P. A., Nokes, D. J. & Medley, G. F. The transmission dynamics of groups A and B human respiratory syncytial virus (hRSV) in England & Wales and Finland: seasonality and cross-protection. *Epidemiol. Infect.* **133**, 279–289 (2005).
47. Mlinaric-Galinovic, G. et al. Analysis of biennial outbreak pattern of respiratory syncytial virus according to subtype (A and B) in the Zagreb region. *Pediatr. Int* **54**, 331–335 (2012).
48. Mufson, M. A., Belshe, R. B., Örvell & Norrby, C. E. Respiratory syncytial virus epidemics: variable dominance of Subgroups A and B strains among children, 1981–1986. *J. Infect. Dis.* **157**, 143–148 (1988).
49. Furlow, B. Triple-demic overwhelms paediatric units in US hospitals. *Lancet Child Adolesc. Health* **7**, 86 (2023).
50. Viñeta Paramo, M. et al. Respiratory syncytial virus epidemiology and clinical severity before and during the COVID-19 pandemic in British Columbia, Canada: a retrospective observational study. *Lancet Reg. Health Am.* **25**, 100582 (2023).
51. Hamid, S. et al. Seasonality of respiratory syncytial virus - United States, 2017-2023. *MMWR Morb. Mortal. Wkly Rep.* **72**, 355–361 (2023).
52. Rhedin S., et al. Correction: Respiratory viruses in hospitalized children with influenza-like illness during the H1n1 2009 pandemic in Sweden. *PLoS One*. 2013;8. https://doi.org/10.1371/annotation/fcd5bca6-cbc4-493e-9083-d11903bcbc48.
53. Bennet, R. et al. Influenza epidemiology among hospitalized children in Stockholm, Sweden 1998–2014. *Vaccine* **34**, 3298–3302 (2016).
54. Paireau, J., Chen, A., Broutin, H., Grenfell, B. & Basta, N. E. Seasonal dynamics of bacterial meningitis: a time-series analysis. *Lancet Glob. Health* **4**, e370–e377 (2016).

55. Shi, J., Wang, X., Ci, F. & Liu, K. Spatiotemporal characteristics and patterns of the COVID-19 pandemic in China: An empirical study based on 413 cities or regions. *Int J. Environ. Res. Public Health* **19**, 2070 (2022).
56. Weinberger, D. M. et al. Impact of the 2009 influenza pandemic on pneumococcal pneumonia hospitalizations in the United States. *J. Infect. Dis.* **205**, 458–465 (2012).
57. Viboud, C. et al. Synchrony, waves, and spatial hierarchies in the spread of influenza. *Science* **312**, 447–451 (2006).
58. Grenfell, B. T., Bjørnstad, O. N. & Kappey, J. Travelling waves and spatial hierarchies in measles epidemics. *Nature* **414**, 716–723 (2001).

Acknowledgements

This work was supported by a grant from the National Institutes of Health (R01AI137093) awarded to D.M.W. The content is solely the responsibility of the authors and does not necessarily represent the official views of the National Institutes of Health. We thank Margareta Eriksson and Rutger Bennet from the Pediatric Infectious Disease Department at Astrid Lindgren Children's Hospital, Karolinska University Hospital, in Stockholm, Sweden, for collecting clinical data on Influenza and RSV epidemics in Stockholm.

Author contributions

K.L. conducted the analyses and wrote both the initial and revised manuscripts. J.H. and A.N. provided data and content expertise and assisted with the response letters to reviewers. D.M.W. and V.E.P. provided content expertise, supervision, and oversaw the analyses for both the initial and revised manuscripts. All authors contributed to drafting and approved the final version of the manuscript.

Competing interests

DMW has received consulting fees from Pfizer, Merck, and GSK, unrelated to this manuscript, and has been PI on research grants from Pfizer and Merck to Yale, unrelated to this manuscript. The remaining authors declare no competing interests.

Additional information

Supplementary information The online version contains supplementary material available at https://doi.org/10.1038/s41467-025-63654-1.

Correspondence and requests for materials should be addressed to Ke Li.

Peer review information *Nature Communications* thanks the anonymous reviewers for their contribution to the peer review of this work. A peer review file is available.